AIAA JOURNAL
Vol. 46, No. 2, February 2008

Dislocation-Based Plasticity for Impact Loading in Solids

Xia Lu*
University of Florida, Shalimar, Florida 32579
and
Sathya V. Hanagud†
Georgia Institute of Technology, Atlanta, Georgia 30309

DOI: 10.2514/1.26354

In this paper, a dislocation-based plasticity model is formulated in the framework of continuum mechanics and nonequilibrium thermodynamics for solids under high strain rates. Specifically, the formation of a dislocation network behind the shock front, associated plastic flow, resulting heating due to plastic work, and evolution of the morphology of the polycrystalline structure are modeled. The associated changes of dynamic strength or yield stress with the increasing shock strength due to nucleation of dislocations at the shock front are modeled. The microstructural characteristics of the dislocation network are modeled by selected internal state variables. The irreversible nonequilibrium processes at high strain rates are modeled by selected nonequilibrium state variables and their evolution equations. The results clearly show the increased localized heating due to increased dynamic strength and the associated plastic flow.

Nomenclature

$B^{(\alpha)}_{\text{drag}}$	=	viscous drag coefficient
$b^{(\alpha)}$	=	magnitude of Burgers's's vector
$b^{(\alpha)}_i$	=	Burgers's vector for slip system (α), $b^{(\alpha)}s^{(\alpha)}_i$
E_L	=	average dislocation line energy
G	=	average shear modulus of the lattice
e	=	specific internal energy
f	=	specific Helmholtz's free energy
G_{ijkl}	=	shear modulus
J^s_i	=	entropy flux
$J^{(\alpha)}_{ij}$	=	dislocation flux tensor
$K^{(\alpha)}$	=	total source for changing of the dislocation density
$K^{(\alpha)}_J$	=	rate of changing of the dislocation density by the dislocation reaction
$K^{(\alpha)}_m$	=	rate of dislocation multiplication
$K^{(\alpha)}_n$	=	rate of dislocation nucleation at the shock front
k_{ij}	=	heat conduction coefficients
$k^{(\alpha)}_d$	=	resistance of dislocation motion for slip system (α)
$m^{(\alpha)}_i$	=	unit vector of gliding direction of slip system (α)
$n^{(\alpha)}_i$	=	unit vector normal to the slip plane of slip system (α)
q_i	=	heat flux
s	=	specific entropy
$s^{(\alpha)}_i$	=	unit vector of Burgers's vector for slip system (α)
t_q	=	relaxation time for heat propagation
t_σ	=	viscous relaxation time
$t^{(\alpha)}_d$	=	relaxation time for the dislocation motion of slip system (α)
V_{ij}	=	rate of deformation
V^e_{ij}	=	rate of elastic deformation
V^{plastic}_{ij}	=	rate of plastic deformation
v_i	=	velocity
$v^{(\alpha)}$	=	dislocation motion of slip system (α)
$Z^{(\alpha)}_{ij}$	=	orientation tensor of slip system (α), $Z^{(\alpha)}_{ij} = s^{(\alpha)}_i n^{(\alpha)}_j$
α_d	=	nondimensional thermal softening coefficient
Γ_i	=	rate of change of the characteristic angle
Δ_L	=	average distance between the two closest dislocation segments
η_{ijkl}	=	viscous modulus
η^s	=	rate of entropy production
θ	=	absolute temperature
ρ	=	density
ρ_d	=	total dislocation density
$\rho^{(\alpha)}_d$	=	dislocation density of slip system (α)
σ_{ij}	=	stress tensor
σ^e_{ij}	=	equilibrium stress tensor
σ^{ne}_{ij}	=	nonequilibrium stress tensor
ρ_{d0}	=	reference dislocation density
$\rho_{d\text{-HP}}$	=	threshold value of dislocation density for hardening
$\varsigma^{(\alpha)}$	=	nondimensional effective coefficient
$\tau_{c\theta}$	=	reference stress for softening
$\tau_{c\rho}$	=	reference stress for hardening
τ_{cr0}	=	yielding stress at $\rho_d = \rho_{d0}$
$\tau^{(\alpha)}_{\text{drag}}$	=	electron and phonon drag in slip system (α)
$\tau^{(\alpha)}_{\text{eff}}$	=	local resolved shear stress acting on dislocation segments in slip system (α)
$\tau^{(\alpha)}_{\text{ext}}$	=	external (or long-range) shear stress resolved on slip system (α)
$\tau^{(\alpha)}_{\text{fri}}$	=	intrinsic lattice resistance in slip system (α)
$\tau^{(\alpha)}_{\text{int}}$	=	internal shear stress due to morphological configuration of dislocation segments in slip system (α)
$\chi^{(\alpha)}_D$	=	fraction of the average stored interface energy that contributes to the *formation* of dislocation segments of slip system (α)
$\chi^{(\alpha)}_L$	=	average fraction of plastic work done on the formation of dislocation segments of slip system (α)
Ω_{ij}	=	spin tensor
$\Omega^{\text{plastic}}_{ij}$	=	plastic spin tensor
ω_i	=	spin vector

Received 6 July 2006; revision received 17 July 2007; accepted for publication 17 July 2007.

*Visiting Assistant Professor, Research and Engineering Education Facility, 1350 North Poquito Road. Senior Member AIAA.

†Professor, School of Aerospace Engineering, 270 Ferst Drive. Fellow AIAA.

Subscripts

i, j, k, l, m, n = vector or tensor indices and Einstein's summation convention

I. Introduction

NOSE erosion and heat-affected zones (HAZ) at the tip of projectiles are observed during impact and penetration of metallic kinetic projectiles into hard targets [1,2]. This may lead to undesirable degradation of the performance of the projectiles. In the past, issues of thermomechanical dissipations have been addressed in different frameworks of thermodynamics. The very early work of Zener [3] considered thermoelastic dissipation. The associated phenomenon is described as the Thomsom effect. When a solid is stressed adiabatically, the mechanical and thermal fields are coupled. Irreversible heat conduction occurs and entropy is produced when mechanical energy is converted into heat. Boley and Weiner [4] pointed out the significant contribution of thermoelastic dissipation to the damping of vibrations. Many authors have extended Zener's [3] analysis. Examples include the work of Bishop and Kinra [5] and Bishop et al. [6]. In these works, thermoelastic dissipation is formulated in the framework of classical irreversible thermodynamics (CIT). Thermoviscoplastic dissipation consists of three different kinds of dissipation mechanisms: thermoelastic, viscous, and plastic dissipations. Unlike the thermoelastic dissipation, viscous and plastic dissipations are inelastic processes, which correspond to irreversible mechanical deformations. Several models for thermoviscoplastic processes have been developed in the framework of rational thermodynamics by using the internal variable theory [7–12]. In the study by Rosakis et al. [8], the fraction of the rate of plastic work converted into heating and cold work is examined at low and medium strain rates (10^{-3} s^{-1} to 1 s^{-1} and 10^{3} s^{-1} to 10^{4} s^{-1}).

This paper, however, is addressed to the problem of heating of the tip of a projectile that impacts and penetrates a hard target. In particular, the model considers the effect of shock waves, high strain rates, the formation of dislocations behind the shock front [13], a pileup of these dislocations [14], the increase in the dynamic strength, the interaction between dislocations, a release of these dislocations, and the following increase of temperature. The plasticity model in this paper is based on dislocation dynamics and then formulated to the evolution of a dislocation network behind the shock front, the associated bulk plastic flow, resulting heating and softening due to plastic work, evolution of morphology of the polycrystalline structure, and the associated increased dynamic strength behind a shock wave. In comparison with the previous works, the model combines the use of equilibrium thermodynamic state variables, internal state variables, and extended nonequilibrium state variables [15,16]. In other words, we proposed a hybrid framework of extended irreversible thermodynamics and internal variable theory to formulate thermoviscoplastic dissipation at high strain rates. A brief introduction to various frameworks of irreversible thermodynamics and a discussion on the necessity of introducing a hybrid framework are first given in the following sections.

A. Framework of Irreversible Thermodynamics

The first framework of irreversible thermodynamics is CIT, which naturally adapted the concept of state from a global description of a continuum in thermostatics to a local description of material point in the continuum. In addition to the classical set of state variables, Onsager et al., in the 1930s, introduced thermodynamic fluxes to describe irreversible processes. At any instant, thermodynamic fluxes instantaneously respond to the generalized forces by a linear relation that holds the Onsager–Casimir reciprocal principle. These thermodynamic fluxes are not considered as additional state variables and therefore do not appear in state functions such as internal energy, free energy, etc., as defined in thermostatics.

In the 1960s, another framework, rational thermodynamics (RT), was introduced by Truesdell et al. In RT, materials are assumed to have memory. This means that at any given instant, dependent variables cannot be determined by only instantaneous values of independent variables, but by their entire histories. In RT, complementary variables (such as internal energy, heat flux, stress tensor and entropy) are related to the entire history of independent variables (such as deformation and temperature) by functional relationships. To reduce the RT representation and avoid the use of functional equations, Bridgeman first proposed an introduction of "a large-scale thermodynamic parameter of state." These state parameters, which extend the state space of CIT and RT, are called the internal (state) variables. Physically, internal variables represent some microscopic material structural characteristics or their ensemble characteristics. For example, for materials of structural damages such as microcracks, damage content tensor can be introduced as internal variables to supplement the description of a local equilibrium state in addition to the deformation and temperature. Internal variables are independent variables and obey a special rate equation [7]. These internal variables are "hidden" in the sense that their rate equations are local (i.e., spatially independent) and can be directly integrated. In the internal variable theory (IVT), the dissipation (or internal power) induced by an internal variable is equal to the product of its rate of change and the corresponding conjugated force. The introduction of internal variables can be beneficial when selected material structural characteristics and their associated dissipations affect the local properties significantly. However, other than the rate of change of an internal variable, irreversible processes associated with the evolutions of relevant material structural characteristics have to be considered. For example, irreversible processes such as the motions of microcracks and evolution of a microcrack network, other than the rate of change of damage content tensor, are also crucial. To measure these irreversible processes, thermodynamic fluxes as in CIT are needed.

CIT and IVT have gone beyond equilibrium thermodynamics. However, they are limited to the validation of the fundamental hypothesis, which assumes that there exists or accompanies a local equilibrium state. The applicability of the assumption of local equilibrium state relies on the validation of Boltzmann's distribution. This restricts CIT and IVT only to the applicable cases that are only slightly fluctuated to Boltzmann's distribution and therefore not far away from thermodynamic equilibrium. The sufficient condition for the validity of the local equilibrium assumption is that all of the associated thermodynamic processes relax fast enough in comparison with some characteristic times of interest. For processes that have relaxation times much larger than dynamic characteristic times of interest, they are away from thermodynamic equilibrium. However, they can be considered "locked" in a nearly equilibrium state at every instant. For processes that have relaxation times much smaller than dynamic characteristic times of interest, they can be considered as instantaneous responses, as in CIT. In these two situations, the assumption of a local equilibrium state is valid. However, in many cases, the characteristic relaxation times of the involved irreversible dissipation processes, either chemical, mechanical, thermal, or electrical, can be at the same order of dynamic characteristic times of interest. Therefore, at any instant during these processes, every point in the continuum is at a state that is far away from thermodynamic equilibrium. The assumption of a local equilibrium state is no longer applicable.

Extended irreversible thermodynamics (EIT) relaxes the restriction of the assumption of a local equilibrium state by introducing a primitive concept of a local nonequilibrium state. Therefore, a local nonequilibrium state, which allows for a description of a state far away from thermodynamic equilibrium, is assigned to every material point in a continuum at any instant [15,16]. EIT constructs a nonequilibrium state space in the following way. In addition to the classical set of equilibrium state variables, an extended set of nonequilibrium state variables is introduced to complement the description of a local nonequilibrium state. These extended nonequilibrium state variables are also called thermodynamic fluxes, which are fast and nonconserved variables. Every irreversible dissipative process, either macroscopic (related to

classical state variable) or microscopic (related to internal state variable), possesses an associated thermodynamic flux, which can be used to describe some types of interaction of a material point with its neighborhood. Each flux is activated by the spatial gradients of either a classical state variable or an internal state variable and therefore is spatially correlated. In contrast to the internal state variables, these thermodynamic fluxes are independent nonlocal state variables. In contrast to thermodynamic fluxes in CIT, these thermodynamic fluxes have relaxation characteristics and therefore directly contribute to state functions. These nonequilibrium contributions can be significant when relaxation times of thermodynamic fluxes are not negligible. In EIT, nonequilibrium state functions such as entropy, free energy, and internal energy are functions of the entire set of state variables, including both equilibrium and nonequilibrium variables. Furthermore, entropy flux depends on all thermodynamic fluxes, not just on heat flux as in the framework of CIT, RT, or IVT. From the second law of EIT, the rate of entropy production is strictly non-negative to ensure the evolution direction of irreversible processes. This also imposes restrictions on the constitutive relations and evolution equations of thermodynamic fluxes.

B. Dislocation-Based Plasticity Model in a Hybrid Framework

Modeling of the complicated material behaviors needs to incorporate underlying multiscale material structural characteristics. A polycrystalline solid such as a metallic projectile can possess structural characteristics at various scales: crystal lattice at the atomic scale, morphology of grains and phases at the mesoscale level, and defects at various scales. For impact and penetration problems, among various material structural characteristics, the most significant contribution to thermoviscoplastic dissipation is by a dislocation network. Therefore, a dislocation-based plasticity model is very beneficial to represent the evolution of a dislocation network and the consequent organization or patterning of dislocation and to interpret the consequent heating, hardening, and localization. To depict a dislocation network, internal state variables are natural choices for this purpose.

On the other hand, for high-speed impact and penetration problems, the pertinent characteristic times t_{ch} of interest are associated with some meso, micro, and macro phenomena (e.g., formations of heat-affected zones, shear bands, and shock fronts). Then t_{ch} is on the order of the time that is needed for the shock wave front to travel through the corresponding length scales: HAZ are $20 \sim 100$ μm, shear bands are $1 \sim 50$ μm, and the thickness of the shock front is $\sim\mu$m. This leads to a broad range of characteristic time scales (e.g., $t_{\text{ch}} = 10^{-11} \sim 10^{-7}$ s). Usually, the thermal propagation and dislocation evolution processes have shorter characteristic times than those of viscous processes. However, the relaxation times of these processes all have comparable t_{ch}. Thus, the evolutions of these processes have to be modeled under a proper thermodynamics framework such as EIT. The relaxation time for the evolution of the dislocation network is a much more complicated issue. The long-range and short-range interactions between dislocations and the various drag effects compete with each other. Each of these possesses a different relaxation mechanism. Therefore, each dislocation segment in a slip system can have its own relaxation time. However, an averaged relaxation time over all the belonging dislocation segments is assigned to every slip system. The relaxation time of the slip system is assumed to be on the order of the time for the shock wave traveling through a shear band or a HAZ (i.e., 10^{-10} s $\sim 10^{-7}$ s for steels).

In this paper, the dislocation network is assumed to consist of a finite number of discrete slip systems. Each slip system (α) is described by two internal state variables: its characteristic orientation tensor $Z_{ij}^{(\alpha)}$ (i.e., the Schmid orientation tensor) and an associated scalar quantity, dislocation density $\rho_d^{(\alpha)}$, for the collective length of dislocation segments in slip system (α). A vector quantity [the dislocation motion $v^{(\alpha)}$ denotes the gliding velocity of slip system (α)] is introduced as an extended state variable associated with the dislocation network. The complete formulation consists of the equations of conservation constitutive relations, including both equilibrium and nonequilibrium relations, and the derivation for the expression of the specific internal energy. The derivation is based on the evolution equation of entropy, constitutive relations, and the first and second laws of thermodynamics.

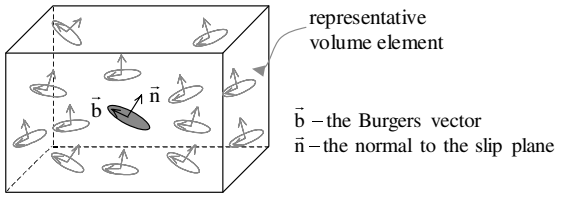

Fig. 1 Slip systems in an infinitesimal volume at x_i.

II. Plasticity Model Based on Dislocation Dynamics

In general, it is necessary to consider a probabilistic distribution of dislocation segments in the space. To understand the physics of the problem, the heating of the solid due to plastic work, and possible phase transitions in the solid, a deterministic distribution of dislocation segments is first considered. An infinitesimal volume at a spatial coordinate $\boldsymbol{x}$ is considered. The volume element contains a number of discrete dislocation segments, as shown in Fig. 1. These dislocation segments are classified by the active slip systems. A slip system, denoted by an upper index (α), is characterized by two vectors: the vector $n_i^{(\alpha)}$ normal to the slip plane and Burgers's vector [17] $b_i^{(\alpha)} = b^{(\alpha)} s_i^{(\alpha)}$, where $b^{(\alpha)}$ is the magnitude of Burgers's vector and $s_i^{(\alpha)}$ the associated vector for slip direction. Then a second-order tensor, called the Schmid orientation tensor $Z_{ij}^{(\alpha)} = s_i^{(\alpha)} n_j^{(\alpha)}$, is assigned to each slip system (α) [18,19]. Each dislocation segment possesses a characteristic length that is the length of the dislocation line.

For a given slip system, the ensemble behavior of dislocations is obtained by a simple summation. In this way, a scalar density $\rho_d^{(\alpha)}$ for slip system (α) is defined as the collective length of dislocation segments that belong to slip system (α) per unit volume. The motion of the slip system (α) is denoted by $v_i^{(\alpha)}$, which is the averaged velocity of dislocation segments that belong to slip system (α). We denote the vector $v_i^{(\alpha)} = v^{(\alpha)} m_i^{(\alpha)}$, where $v^{(\alpha)}$ is the magnitude of gliding velocity and $m_i^{(\alpha)}$ is the gliding direction. Obviously, $\rho_d^{(\alpha)}$ and $v^{(\alpha)}$ are the field variables that are functions of space and time, and $\rho_d^{(\alpha)}$ and $v^{(\alpha)}$ are chosen as the internal state variables and the thermodynamic flux associated with the dislocation evolution processes, respectively. During the finite deformation processes, the characteristic orientation of crystal lattice can distort. Then the orientation of slip system $Z_{ij}^{(\alpha)}$ that is attached to the crystal lattice also evolves with time. Thus, the Schmid orientation tensor $Z_{ij}^{(\alpha)}$ is also be considered as an internal state variable.

In general, (α) is a random variable and can vary from 0 to 2π. The associated distribution can be described by an orientation probability distribution. To keep the model simple and deterministic, it is assumed that only a finite number of α are possible. A model with a probability distribution was also formulated and will be presented in a separate paper. The finite number of α is assumed to account for the possible slip systems. It is further assumed that every location has the same set of representative slip systems. This is a very restrictive assumption but will provide a deterministic model. The resulting dislocation flux tensor $J_{ij}^{(\alpha)}$ of slip system (α) is

$$J_{ij}^{(\alpha)} = \rho_d^{(\alpha)} b^{(\alpha)} v^{(\alpha)} Z_{ij}^{(\alpha)} \tag{1}$$

The lower indices other than i, j, k, l, m, and n do not indicate the coordinate indices. The rate of plastic deformation is the symmetric part of the ensemble of dislocation flux tensor over all the slip systems. Therefore,

$$V_{ij}^{\text{plastic}} = \frac{1}{2}\sum_{\alpha}\left(J_{ij}^{(\alpha)} + J_{ji}^{(\alpha)}\right) = \frac{1}{2}\sum_{\alpha}\rho_d^{(\alpha)} b^{(\alpha)} v^{(\alpha)}\left(Z_{ij}^{(\alpha)} + Z_{ji}^{(\alpha)}\right) \tag{2}$$

The plastic spin is an antisymmetric part of the ensemble of the dislocation flux tensor over all the slip systems.

$$\Omega_{ij}^{\text{plastic}} = \frac{1}{2}\sum_{\alpha}\left(J_{ij}^{(\alpha)} - J_{ji}^{(\alpha)}\right) = \frac{1}{2}\sum_{\alpha}\rho_d^{(\alpha)} b^{(\alpha)} v^{(\alpha)}\left(Z_{ij}^{(\alpha)} - Z_{ji}^{(\alpha)}\right) \quad (3)$$

Dislocation dynamics describes the evolution of a dislocation network. It consists of the dislocation evolutions and the dislocation motions, which depend on each other. During their motion, dislocation segments interact with each other via long-range forces and also undergo short-range reactions. It leads to the destruction (e.g., annihilation), multiplication/nucleation, reorientation and immobilization (e.g., hardening and dislocation wall) of the reacting dislocation segments, and dislocation patterning (e.g., kink and twinning). All of these phenomena result in heterogeneous plastic flow and the associated localization phenomena in crystals at mesoscale.

A. Dislocation Evolution and Contributions of Shock Loading

The dislocation segments in a slip system can be created or destroyed by dislocation nucleation, dislocation multiplication, and dislocation reactions. In this paper, we specifically study the dislocation nucleation behind the shock wave. The corresponding source term is related to an increase of the dynamic strength. Following IVT, the general form of the evolution equation of dislocation density of slip system (α) can be formulated as follows.

$$\frac{\partial \rho_d^{(\alpha)}}{\partial t} + \frac{\partial}{\partial x_k}\left(\rho_d^{(\alpha)} v_k\right) = K^{(\alpha)} \quad (4)$$

The first term on the left-hand side is the rate of change of dislocation density of slip system (α), and the second term is the convection of dislocation segments through mass convection. The term on the right-hand side is the source term $K^{(\alpha)}$. The source contains three contributions due to dislocation nucleation by shock loading $K_n^{(\alpha)}$, dislocation multiplication $K_m^{(\alpha)}$, and dislocation reaction $K_J^{(\alpha)}$.

$$K^{(\alpha)} = K_n^{(\alpha)} + K_m^{(\alpha)} + K_J^{(\alpha)} \quad (5)$$

During the deformation processes at low strain rates, the resolved shear stress for homogeneous dislocation nucleation (i.e., embryos nucleation from pure crystal) is very high, several orders higher than the yield stress [20]. Therefore, dislocation nucleation occurs mainly in the regions that have stress concentration, such as at all kinds of interfaces. At the shock fronts, a lattice interface is generated by the sharp gradient of rate of the deformation. This interface becomes a bed for dislocation nucleation. By improving Smith and Hornbogen's models, Meyers [13] proposed a homogeneous dislocation nucleation for the shock wave: dislocations are homogeneously nucleated at or close to the shock front by the shear stress, these dislocations move short distances at subsonic speeds, and new dislocation interfaces are generated behind the shock front. The dislocation density at the interface depends on the difference in specific volume between the two lattices. In this paper, these concepts are translated into a mathematical formulation as follows. At shock fronts, a lattice mismatched interface is generated and of high elastic strain energy. As the shock becomes stronger, this rate of elastic strain energy $W(\sigma_{ij})$ becomes larger than some critical level W_{cr}. Then a large number of misfits create dislocation nucleation at this interface. The shock front is indicated by a sharp stress gradient. Then

$$K_n^{(\alpha)} = \begin{cases} \frac{\chi_D^{(\alpha)}}{E_L} W(\sigma_{ij}) & W(\sigma_{ij}) > W_{\text{cr}} \text{ and at the shock front} \\ 0 & \text{otherwise} \end{cases} \quad (6)$$

where $\chi_D^{(\alpha)}$ is the fraction of the average stored interface energy that contributes to the formation of dislocation segments (α). The threshold quantity W_{cr} in this paper is extended to vary with shock strength. Then the rate of accumulation of dislocations becomes dependent on shock strength. The quantity W_{cr} is assumed to gradually increase with the increasing shock intensity to avoid an avalanche of dislocation nucleation at strong shocks. Thus,

$$W_{\text{cr}} = W_{\text{cr}}(P) \quad (7)$$

where P is the peak shock pressure. For dislocation multiplication $K_m^{(\alpha)}$, we used a phenomenological model by Hähner [21] based on the Frank–Reed hypothesis. For dislocation creation and annihilation by dislocation reaction $K_J^{(\alpha)}$, we have adapted the formulation by Zaiser [22] and El-Azab [23]. The details for the corresponding formulation can be referred to in Appendix A. From Eqs. (A1–A5), we can see that the sources for the evolution of dislocation density, due to multiplication and reaction, rely on the corresponding dislocation motion, which is not triggered until the resolved stress reaches critical values. Therefore, at low strain rates, dislocation density only increases dramatically after yielding and will not change if there is no plastic flow.

B. Dislocation Motion

The motion of slip system (α) is driven by the local resolved shear stress $\tau_{\text{eff}}^{(\alpha)}$. It comprises four parts: the external (long-range) shear stress resolved on slip system (α), $\tau_{\text{ext}}^{(\alpha)}$; the internal shear stress due to the morphological configuration of dislocation segments such as dislocation self-interactions and short-range interaction with the obstacles, $\tau_{\text{int}}^{(\alpha)}$; the intrinsic lattice resistance, including temperature-dependent Pierels resistance, $\tau_{\text{fri}}^{(\alpha)}(\theta)$; and the electron and phonon drag, $\tau_{\text{drag}}^{(\alpha)}(\theta)$ [22–25]; that is,

$$\tau_{\text{eff}}^{(\alpha)} = \tau_{\text{ext}}^{(\alpha)} - \tau_{\text{int}}^{(\alpha)} - \tau_{\text{drag}}^{(\alpha)} - \tau_{\text{fri}}^{(\alpha)} \quad (8)$$

The detailed discussion and formulation for each term in the preceding equation can be referred to in Appendix B. The avalanche occurrence of dislocation motions of a slip system implies a critical yielding condition. At zero stress, the dislocation relaxes into some local equilibrium configuration in which the external and internal stresses balance with each other. With the increase of external stresses, the number of dislocation segments, which move to a new equilibrium configuration, increases. When the local resolved external load $\tau_{\text{ext}}^{(\alpha)}$ reaches some critical value $\tau_{\text{ext,cr}}$, a significant amount of dislocation motion would appear that corresponds to macroscopic plastic yielding phenomena. Following EIT, we can formulate that the dislocation motion $v^{(\alpha)}$, as the thermodynamic flux of dislocation evolution, follows the first-order relaxation with the resolved effective stress as the source.

$$\begin{cases} t_d^{(\alpha)} \frac{\mathrm{D}v^{(\alpha)}}{\mathrm{D}t} = -v^{(\alpha)} + \frac{1}{k_d^{(\alpha)}(\theta)} \tau_{\text{eff}}^{(\alpha)} & \text{if } \tau_{\text{ext}}^{(\alpha)} > \tau_{\text{ext,cr}} \\ v^{(\alpha)} = 0 & \text{otherwise} \end{cases} \quad (9)$$

where $t_d^{(\alpha)}$ is the relaxation time of dislocation motion. This relaxation of dislocation motion correlates to the relaxation of drag effects. Therefore, $t_d^{(\alpha)}$ depends on the relaxation time of the dominant drag effects. For metals, the order of $t_d^{(\alpha)}$ is assumed to be comparable to the characteristic time scales of the high-rate dynamic processes such as the shock wave traveling through the dislocation network in a infinitesimal volume. The coefficient $k_d^{(\alpha)}$ is the resistance to dislocation motion, which decreases with the increase of temperature and represents a thermal softening effect (e.g., a model similar to the thermal softening factor in the Johnson–Cook model is employed).

$$k_d^{(\alpha)}(\theta) = k_d^{(\alpha)}(\theta_0)\left(1 + \alpha_d \frac{\Delta\theta}{\theta_0}\right)^{-1} \quad (10)$$

where α_d is the nondimensional thermal softening coefficient, and θ_0 the reference temperature. There are some other power law relations applied for applied stresses and the dislocation gliding velocity [20]. The order of power changes with the temperature and magnitude of

the dislocation velocity. However, because we count in the internal stress source that changes with dislocation density in $\tau_{\text{eff}}^{(\alpha)}$ and temperature dependence in $k_d^{(\alpha)}$, the first-order relaxation equation (9) is assumed to be sufficiently accurate.

The critical stress $\tau_{\text{ext,cr}}$ depends on the average dislocation density ρ_d, which agrees with the strain-rate hardening effects that are caused by dislocation pileups, and also depends on the temperature. A phenomenological formulation of $\tau_{\text{ext,cr}}$ is given by

$$\tau_{\text{ext},c} = \tau_{\text{cr0}} + \tau_{c\rho}\sqrt{\frac{\rho_d}{\rho_{d0}} - 1} + \tau_{c\theta}\left(\frac{\theta}{\theta_0} - 1\right) \tag{11}$$

The subscript 0 indicates a reference state, τ_{cr0} is the reference yielding stress at ρ_{d0}, and $\tau_{c\theta}$ and $\tau_{c\rho}$ are some constant reference stresses for hardening and softening, respectively. As dislocations pile up, the slip systems change to a denser configuration and therefore the mobility of slip systems reduces; in other words, the critical stress increases. Because dislocation pileup or nucleation at the shock front depends on shock strength, the dynamic strength or yield stress becomes dependent on shock strength through the Hall–Petch hardening effect. However, at the early stage of dislocation pileup, this hardening effect is not obvious and can be assumed to be negligible. Only up to some level of dislocation pileup, denoted by some threshold value $\rho_{d\text{-HP}}$, is the hardening counted. In a mathematical form,

$$\tau_{c\rho} = \begin{cases} 0 & \rho_d < \rho_{d\text{-HP}} \\ \tau_{c\rho 0} & \rho_d \geq \rho_{d\text{-HP}} \end{cases} \tag{12}$$

because at each instant before, during, or after plastic deformation, the state can be distinguished by the corresponding dislocation distribution. Then the future state is totally determined by the current state.

It is noticed that as dislocation segments nucleate and accumulate, the consequent increase of dislocation density will increase the line tension between dislocation segments or increase the magnitude of internal stress, as shown in Eq. (B2). Then the total resolved shear stress decreases. This leads to a reduced dislocation motion [see Eq. (9)]. This also restricts the maximum magnitude of dislocation motion that can be attained. This is consistent with the statement made by Meyers [13]. The dislocation motion is subsonic. It means that the dislocation velocity is less than the elastic shear wave speed.

C. Evolution of the Schmid Orientation Tensor

As stated, the evolution of Schmid orientation tensor $Z_{ij}^{(\alpha)}$ corresponds to the lattice rotation during dynamic deformation processes. The lattice rotation comes from geometric effects, which can be observed at the scale of grains. In a general case, the evolution of $Z_{ij}^{(\alpha)}$ is given by a rate form.

$$\frac{\partial Z_{ij}^{(\alpha)}}{\partial \mathrm{t}} = f(\sigma_{ij}, \rho_d^{(\alpha)}, \vartheta) \tag{13}$$

where ϑ is the factor related to the grain size. In the following derivations, the evolution of lattice rotations is approximately determined by the associated rigid body particle rotation. The rigid body particle rotation is governed by the spin tensor Ω_{ij} [spin tensor $\Omega_{jk} = \frac{1}{2}(v_{i,j} - v_{j,i})$]. A corresponding spin vector can be defined as follows.

$$\omega_i = -e_{ijk}\Omega_{jk} \tag{14}$$

From the Schmid orientation tensor $Z_{ij}^{(\alpha)}$, we can define an angle as

$$\Gamma_i = -\mathrm{e}_{ijk}Z_{jk}^{(\alpha)} \tag{15}$$

where e_{ijk} is a third-order permutation tensor. Then the evolution of $Z_{ij}^{(\alpha)}$ can be given by the rate of change of the angle Γ_i, which is equal to the spin vector ω_i; that is,

$$\frac{\partial \Gamma_i}{\partial \mathrm{t}} = \omega_i \tag{16}$$

III. Constitutive Relations

The constitutive relations are divided into two groups: equilibrium constitutive relations and evolutions of thermodynamic fluxes. In the first group, the instantaneous responses of material are described by the relations between the equilibrium classical state variables or the internal state variables. In the second group, the nonequilibrium responses of material are described by the relaxations of thermodynamic fluxes. We assume that the total stress tensor σ_{ij} consists of an equilibrium stress tensor σ_{ij}^e and a nonequilibrium stress tensor σ_{ij}^{ne} and that the total rate of deformation V_{ij} consists of an elastic part V_{ij}^e and a plastic part V_{ij}^{plastic}.

$$\sigma_{ij} = \sigma_{ij}^e + \sigma_{ij}^{\text{ne}} \tag{17a}$$

$$V_{ij} = V_{ij}^e + V_{ij}^{\text{plastic}} \tag{17b}$$

A. Equilibrium Constitutive Relations

1. *Equilibrium Stress–Strain Relation in Rate Form*

In many shock physics analysis, the hydrostatic pressure takes a special role. The stress tensor is then usually decomposed into a pressure and a deviatoric stress tensor. Similarly, the rate of deformation can also be decomposed. Thus, the equilibrium stress tensor σ_{ij}^e can be split into a pressure P^e and a deviatoric stress tensor σ_{ij}^{ed}.

$$\sigma_{ij}^e = P^e\delta_{ij} + \sigma_{ij}^{ed} \tag{18}$$

where $P^e = \frac{1}{3}\sigma_{ii}^e$, $\sigma_{ij}^{ed} = \sigma_{ij}^e - P^e\delta_{ij}$.

The rate of elastic deformation can also be decomposed in a similar way.

$$V_{ij}^e = \tfrac{1}{3}V_{kk}^e\delta_{ij} + V_{ij}^{ed} \tag{19}$$

where $V_{ij}^{ed} = V_{ij}^e - \frac{1}{3}V_{kk}^e\delta_{ij}$.

In shock physics, the equilibrium stress–strain relations consist of two parts: an equation of state and a deviatoric relation. The rate form of equation of state can be written as

$$\dot{P}^e = A(\rho,\theta)(\tfrac{1}{3}V_{ii}^e) + B(\rho,\theta)\dot{\theta} \tag{20}$$

which is obtained from equation of state $P^e = P^e(\rho,\theta)$. The rate form of deviatoric relation can be written as

$$\overset{\circ}{\sigma}{}_{ij}^{ed} = G_{ijkl}V_{kl}^{ed} \tag{21}$$

where G_{ijkl} is the elastic modulus. In the preceding, the material time derivatives for a 1) vector $\overset{\circ}{a}_i = \dot{a}_i + \Omega_{ij}a_j$ and 2) second-order tensor $\overset{\circ}{A}_{ij} = \dot{A}_{ij} + \Omega_{ij}A_{ji} - A_{ij}\Omega_{ji}$ are used.

2. *Dislocation Evolution*

Dislocation evolution follows Eq. (4).

B. Evolution of Thermodynamic Fluxes

Each irreversible process has an associated thermodynamic flux. All of these thermodynamics fluxes are the extended state variables. It is assumed that the evolution of these thermodynamic fluxes is governed by first-order relaxation equations. The source for their evolutions is the corresponding generalized force, which is usually the spatial gradient of classical state variables. The couplings between different irreversible processes are assumed to be small and are not considered herein.

1. Evolution of Nonequilibrium Stresses

The viscous effect is found to be important even in fast processes such as shock waves. For metallic materials in solid phases, the viscous mechanisms are associated with viscous lattice stretching, viscous slips of phase, grain boundaries, etc. For metallic materials in the liquid phase, the viscous mechanism comes from viscous flow. The viscous dissipation becomes dominant. The corresponding generalized force is the elastic strain rate V^e_{ij}. The relaxation time of viscous process is denoted by t_σ. The equation of evolution for nonequilibrium stress is given by

$$t_\sigma\left(\overset{\circ}{\sigma^{\text{ne}}_{ij}}\right) = -\sigma^{\text{ne}}_{ij} + \eta_{ijkl}V^e_{kl} \tag{22}$$

2. Evolution of Heat Flux

A relaxation time denoted by t_q is used for the evolution of heat flux. The generalized force is the temperature gradient $\theta_{,i}$. The evolution for heat flux is governed by

$$t_q\overset{\circ}{q_i} = -q_i - k_{ij}\frac{\partial\theta}{\partial x_j} \tag{23}$$

3. Equation of Dislocation Motion

The motion of dislocations is described by Eq. (9).

IV. Conservation Equations

Balance equations for mass, linear momentum, and energy are as follows.

$$\frac{\mathrm{D}\rho}{\mathrm{D}t} + \rho\frac{\partial v_k}{\partial x_k} = 0 \tag{24}$$

$$\rho\frac{\mathrm{D}v_i}{\mathrm{D}t} - \frac{\partial\sigma_{ik}}{\partial x_k} = \rho f_i \tag{25}$$

$$\rho\frac{\mathrm{D}e}{\mathrm{D}t} + \frac{\partial q_i}{\partial x_i} - \sigma_{ij}V_{ij} = 0 \tag{26}$$

The expression of state function (i.e., the specific internal energy e) is derived in Sec. VI to complete the formulation.

V. Entropy, Second Law of Thermodynamics, and State Functions

A. Entropy Evolution

In EIT, the evolution equation of entropy is given by

$$\rho\frac{\mathrm{D}s}{\mathrm{D}t} + \frac{\partial J^s_i}{\partial x_i} - \eta^s = 0 \tag{27}$$

where the entropy flux J^s_i is assumed to be a function of all thermodynamic fluxes. It is

$$J^s_i = J^s_i\left(\theta, \sigma^{\text{ne}}_{ij}, q_i, \rho^{(\alpha)}_d v_i\right) \tag{28}$$

Therefore, the divergence of entropy flux is given by

$$J^s_{i,i} = \Lambda^1_i\theta_{,i} + \Lambda^3_{ij}q_{j,i} + \Lambda^4_{ijk}\sigma^{\text{ne}}_{jk,i} + \sum_\alpha\frac{\varphi^{(\alpha)}(\theta)}{\theta}\rho^{(\alpha)}_d v_{i,i} \tag{29}$$

where

$$\Lambda^1_i = \frac{\partial J^s_i}{\partial\theta}; \qquad \Lambda^3_{ij} = \frac{\partial J^s_i}{\partial q_j}; \qquad \Lambda^4_{ijk} = \frac{\partial J^s_i}{\partial\sigma^{\text{ne}}_{jk}} \tag{30}$$

The last term in Eq. (30) is the entropy flux due to dislocations. The coefficients $\varphi^{(\alpha)}(\theta)$ are related to the change of magnitude of the entropy due to the dislocation flux of slip system (α). Because high temperature results in high dislocation mobility and large entropy change, we assume that $\varphi^{(\alpha)}$ are strongly dependent on temperature $\bar{\theta}$.

B. Second Law of Nonequilibrium Thermodynamics

To satisfy the second law of thermodynamics, the rate of entropy production is non-negative at any instant and at any location.

$$\theta\eta^s = \rho\dot{e} - \rho\dot{f} - \rho s\dot{\theta} + \theta J^s_{k,k} \geq 0 \tag{31}$$

Sufficient conditions to ensure the preceding inequality for all kinds of possible processes are derived (refer to [26]). The following thermodynamic relations are obtained.

Classical equilibrium relations:

$$\begin{aligned}
&\frac{\partial f}{\partial\theta} = -\mathrm{s} - \frac{1}{\bar{\rho}}\left(1 + \sum_\alpha\frac{\varphi^{(\alpha)}\chi^{(\alpha)}_D}{2E_L}\right)A^{-1}(\rho,\theta)B(\rho,\theta)P^e;\\
&\frac{\partial f}{\partial P^e} = \frac{1}{\rho}\left(1 + \sum_\alpha\frac{\varphi^{(\alpha)}\chi^{(\alpha)}_D}{2E_L}\right)A^{-1}(\rho,\theta)P^e; \qquad \frac{\partial f}{\partial\sigma^{ed}_{ij}} = \frac{1}{\rho}G^{-1}_{ijmn}\sigma^{ed}_{mn};\\
&\frac{\partial f}{\partial\rho^{(\alpha)}_d} = -\frac{1}{\rho}\varphi^{(\alpha)}(\theta)
\end{aligned} \tag{32}$$

Nonequilibrium relations:

$$\begin{aligned}
&\frac{\partial f}{\partial\sigma^{\text{ne}}_{ij}} = \frac{1}{\rho}t_\sigma(\eta_{ijmn})^{-1}\sigma^{\text{ne}}_{mn}; \qquad \frac{\partial f}{\partial q_i} = \frac{1}{\rho}t_q\frac{k^{-1}_{ji}}{\theta}q_j;\\
&\frac{\partial f}{\partial v^{(\alpha)}} = \frac{1}{\rho}\left(1 + \frac{\varphi^{(\alpha)}\chi^{(\alpha)}_L}{E_L}\right)t^{(\alpha)}_d k^{(\alpha)}_d b^{(\alpha)}\rho^{(\alpha)}_d v^{(\alpha)}
\end{aligned} \tag{33}$$

Coefficients of divergence of entropy flux:

$$\Lambda^1_i = -\frac{q_i}{\theta^2}; \qquad \Lambda^3_{ij} = \frac{1}{\theta}\delta_{ij}; \qquad \Lambda^4_{ijk} = 0 \tag{34}$$

Further, we obtain the rate of entropy production as follows.

$$\begin{aligned}
\theta\eta^s = {}& \eta^{-1}_{ijkl}\sigma^{\text{ne}}_{ij}\sigma^{\text{ne}}_{kl} + \frac{k^{-1}_{ij}}{\theta}q_i q_j\\
&+ \sum_\alpha\left\{(k^{(\alpha)}_d v^{(\alpha)} + \tau^{(\alpha)}_{\text{int}} + \tau^{(\alpha)}_{\text{fric}})b^{(\alpha)}\rho^{(\alpha)}_d v^{(\alpha)} + \varphi^{(\alpha)}\right.\\
&\left.\times\left(K^{(\alpha)}_J + \frac{\chi^{(\alpha)}_L}{E_L}k^{(\alpha)}_d b^{(\alpha)}\rho^{(\alpha)}_d v^{(\alpha)}v^{(\alpha)}\right)\right\} \geq 0
\end{aligned} \tag{35}$$

The first two terms in Eq. (35) are associated with the mechanical viscous process and the heat propagation process, respectively. The third term in the summation is associated with dislocation dynamics; the first term in the summation is the plastic dissipation by resolved effective stress, internal stresses, and friction and viscous drag stress; and the second term is the cold work on dislocation formation by multiplication and interaction. The non-negativity of $\bar{\eta}^s$ at any situations requires that

$$\eta^{-1}_{ijkl} \geq 0; \qquad k^{-1}_{ij} \geq 0 \tag{36}$$

and the total plastic dissipation by the effective shear stress and back stresses is larger than the stored cold work on dislocation formation. Further, by considering Eqs. (B2–B4) and (9), we conclude that the resistance to dislocation motion and the coefficients for line tension and friction are non-negative.

$$k^{(\alpha)}_d \geq 0; \qquad \varsigma^{(\alpha)} \geq 0; \qquad B^{(\alpha)} \geq 0 \tag{37}$$

By setting the coefficients of line tension and friction and the dislocation formation by interaction to be zero, we can obtain the

lower limit for the fraction of cold work $\chi^{(\alpha)}$ on dislocation multiplication:

$\chi_L^{(\alpha)} \le -(E_L/\varphi^{(\alpha)})$, where the value of $\varphi^{(\alpha)}$ is negative, because the presence of dislocations increases the elastic strain energy.

VI. First Law of Thermodynamics: Energy Balance Equation

The time derivative of internal energy can be derived as discussed in [26] by using constitutive relations and applying the first and second laws of thermodynamics. We also can obtain the energy balance equation as in Eq. (38). The formulation is then completed. The entire set of governing equations includes conservation equations (24), (25), and (38), equilibrium constitutive relations (20), (21), and (4), nonequilibrium constitutive relations (22), (23), and (9), kinematic relations (2), geometric relation (16), and other relations [Eqs. (17a) and (17b)].

$$
\begin{aligned}
&\left[\rho c_p(\theta) - \theta\left(1 + \sum_\alpha \frac{\varphi^{(\alpha)}\chi_D^{(\alpha)}}{E_L}\right)A^{-1}(\rho,\theta)B^2(\rho,\theta)\right]\dot{\theta} \\
&\quad - \rho\theta\frac{\mathrm{D}}{\mathrm{D}t}\left\{\frac{1}{\rho}\left(1 + \sum_\alpha \frac{\varphi^{(\alpha)}\chi_D^{(\alpha)}}{E_L}\right)A^{-1}(\rho,\theta)B(\rho,\theta)\right\}P^e \\
&\quad = -\theta\left(\frac{q_i}{\theta}\right)_{,i} + 2\frac{k_{ji}^{-1}}{\theta}q_j q_i + \frac{1}{\theta}q_j\theta_{,i} + (\eta_{ijmn})^{-1}\sigma_{mn}^{\mathrm{ne}}\sigma_{ij}^{\mathrm{ne}} \\
&\quad - \left(1 + \sum_\alpha \frac{\varphi^{(\alpha)}\chi_D^{(\alpha)}}{E_L}\right)B(\rho,\theta)\frac{1}{3}V_{ii}^e\theta \\
&\quad + \theta^2\sum_\alpha \frac{\partial}{\partial\theta}\left(\frac{\varphi^{(\alpha)}\chi_D^{(\alpha)}}{\theta E_L}\right)\frac{1}{3}P^e V_{ii}^e \\
&\quad + \theta^2\sum_\alpha \frac{\partial}{\partial\theta}\left(\frac{\varphi^{(\alpha)}}{\theta}\right)\left\{\rho_d^{(\alpha)}v_{i,i} - \left(K_m^{(\alpha)} + K_n^{(\alpha)} + K_J^{(\alpha)}\right)\right\} \\
&\quad + \sum_\alpha\left\{k_d^{(\alpha)}v^{(\alpha)} + \theta^2\frac{\partial}{\partial\theta}\left(\frac{\varphi^{(\alpha)}\chi_L^{(\alpha)}}{\theta E_L}\right)\right. \\
&\quad \left.\times\left(-k_d^{(\alpha)}v^{(\alpha)} + \tau_{\mathrm{eff}}^{(\alpha)}\right)\right\}\rho_d^{(\alpha)}v^{(\alpha)}b^{(\alpha)}
\end{aligned}
\tag{38}
$$

where

$$\theta\frac{\partial s}{\partial\theta} = -\theta\frac{\partial^2 f}{\partial\theta^2} = c_p(\theta)$$

We define the specific heat c_p in the framework of nonequilibrium thermodynamics as the heat needed to increase the temperature of system per unit mass by 1 K, with no other processes involved. The specific heat c_p is a function of the temperature.

VII. Numerical Simulations by Finite Difference Method

As observed in the analysis of the recovered penetrators, the HAZ, which appears on the surface of the nose and the shank of the projectile, is limited to a very narrow region. The HAZ thickness is 20 to 100 μm, which is approximately 1/200 of the maximum diameter (e.g., 12.7 mm) of the ogival-nose-shaped penetrator. Consider a surface region R close to the nose tip (Fig. 2a). To study the dynamic deformation processes in region R, we extract two simplified problems according to the assumptions about the mechanisms that take place in the materials in the neighborhood acting on region R. The first problem is a 1-D strain problem. It is assumed that the materials in the neighborhood of region R totally confine the side motions of region R. A 1-D strip with two sides confined is used to characterize region R (see Fig. 2b). At time $t = 0$, a uniform normal stress is applied on the top surface of the strip. The nontrivial velocity component is only in the y direction and is a function of only y and t.

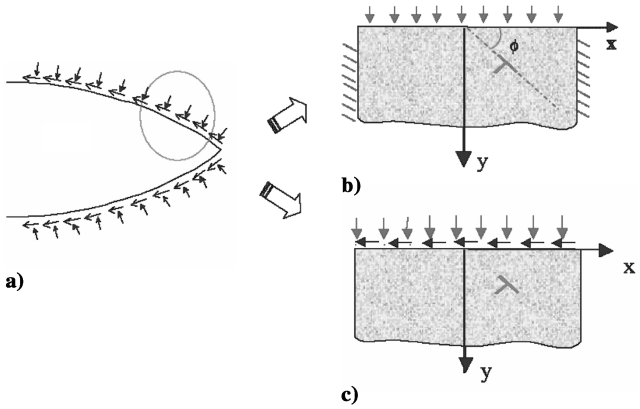

Fig. 2 Simplified problems extracted from the impact and penetration: a) 2-D axisymmetric case, b) 1-D strain case, and c) 2-D half-space case.

The second problem is a 2-D problem. It is assumed that the materials in the neighborhood of region R have no resistance to the side motions of region R. A half-space is used to characterize region R (see Fig. 2c). The surface of the half-space is loaded by a uniform normal stress σ_0 and a uniform shear stress τ_0. The loadings are applied from time $t = 0$. Because there is no constraint on the x direction, the nontrivial stress and strain components are only the yy components. Two velocity components v_x and v_y are functions of only y and t.

Because the constraint imposed by the materials in the neighborhood of region R is between zero and infinity, the real problem, as shown Fig. 2a, is somewhere between the two simplified problems, which will be investigated in a future paper. In this work, for simplicity, only one slip system is assumed (i.e., all the dislocations lie in the direction of ϕ).

A. Finite Difference Technique

For these two problems, all the state variables are functions of y and t. Then we can write the governing equations in the form of the state space as follows.

$$\boldsymbol{A}(U)\frac{\partial U}{\partial t} = \boldsymbol{B}(U)\frac{\partial U}{\partial y} + \boldsymbol{C}(U) \tag{39}$$

where U is the generalized vector that consists of all the state variables. $\boldsymbol{A}(U)$ and $\boldsymbol{B}(U)$ are the corresponding coefficient matrices, and $\boldsymbol{C}(U)$ is the source vector. A two-step Richtmyer finite difference scheme [27–29], which is of a second-order approximation, is employed. The grid is made of N equally separated nodes that are numbered from 1 to N in the y direction. After convergence tests, the spatial step Δy is chosen to be fixed at $\Delta y = 2 \times 10^{-6}$ m, which is enough to resolve for features of HAZ. The considered span is then $(N-1)\,\Delta y = 10^{-3}$ m, which is several tens or hundreds of times the size of HAZ. This gives the number of grid nodes to be 251. The two boundary points are marked as 1 and N. As discussed in the following, the time step Δt will be adjusted at each step to assure stability conditions.

In the two-step finite difference scheme, first the provisional values are calculated at the centers of the rectangular meshes in the y and t planes (i.e., nodes marked by $\times$ in Fig. 3) by a time-forward difference and a centered spatial difference.

$$
\begin{aligned}
U_{j+\frac{1}{2}}^{n+\frac{1}{2}} &= U_{j+\frac{1}{2}}^{n} - \frac{\Delta t}{2\Delta x}A^{-1}\left(U_{j+\frac{1}{2}}^{n}\right)B\left(U_{j+\frac{1}{2}}^{n}\right)\left(U_{j+1}^{n} - U_j^n\right) \\
&\quad + \frac{\Delta t}{2}A^{-1}\left(U_{j+\frac{1}{2}}^{n}\right)C\left(U_{j+\frac{1}{2}}^{n}\right)
\end{aligned}
\tag{40}
$$

where the upper index indicates the time step, and the lower index indicates the spatial step. In Eq. (40), the values at the centers of the t^n border of the rectangular meshes (i.e., nodes marked by $\bigcirc$ in Fig. 3) can be calculated by

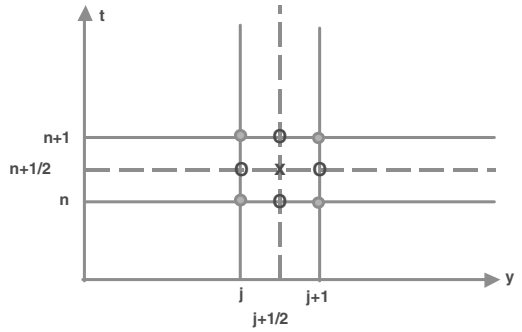

Fig. 3 Spatial and time nodal separation in the Richtmyer finite difference scheme.

$$U^n_{j+\frac{1}{2}} = \tfrac{1}{2}\left(U^n_{j+1} + U^n_j\right) \tag{41}$$

Second, the final values at the corners of t^{n+1} border (i.e., nodes marked by □ in Fig. 3) are obtained by a time-forward difference and a centered spatial difference.

$$U^{n+1}_j = U^n_j - \frac{\Delta t}{\Delta x}A^{-1}\left(U^{n+\frac{1}{2}}_j\right)B\left(U^{n+\frac{1}{2}}_j\right)\left(U^{n+\frac{1}{2}}_{j+\frac{1}{2}} - U^{n+\frac{1}{2}}_{j-\frac{1}{2}}\right) + \Delta t A^{-1}\left(U^{n+\frac{1}{2}}_j\right)C\left(U^{n+\frac{1}{2}}_j\right) \tag{42}$$

In Eq. (42), the values at the centers of the t^{n+1} border of the rectangular meshes (i.e., nodes marked by ○ in Fig. 3) are calculated as follows.

$$U^{n+\frac{1}{2}}_j = \tfrac{1}{2}\left(U^{n+\frac{1}{2}}_{j-\frac{1}{2}} + U^{n+\frac{1}{2}}_{j+\frac{1}{2}}\right) \tag{43}$$

For those state variables that do not have the imposed boundary conditions, a special treatment is needed. According to [29], the boundary technique is important for the finite difference approach. Inappropriate boundary techniques may generate oscillations that cannot be damped and propagate into the interior. The oscillation sometimes overwhelms the real signal. Therefore, some special treatment such as artificial viscosity is introduced to overcome the problem. In this study, the boundary technique for the two-step Richtmyer scheme is employed. The steps can be written as follows.First step:

$$U^{n+\frac{1}{2}}_1 = U^n_1 - \frac{\Delta t}{2\Delta x}A^{-1}(U^n_1)B(U^n_1)(U^n_2 - U^n_1) + \frac{\Delta t}{2}A^{-1}(U^n_1)C(U^n_1) \tag{44a}$$

$$U^{n+\frac{1}{2}}_N = U^n_N - \frac{\Delta t}{2\Delta x}A^{-1}(U^n_N)B(U^n_N)(U^n_N - U^n_{N-1}) + \frac{\Delta t}{2}A^{-1}(U^n_N)C(U^n_N) \tag{44b}$$

Second step:

$$U^{n+1}_1 = U^n_1 - \frac{2\Delta t}{\Delta x}A^{-1}\left(U^{n+\frac{1}{2}}_1\right)B\left(U^{n+\frac{1}{2}}_1\right)\left(U^{n+\frac{1}{2}}_{\frac{3}{2}} - U^{n+\frac{1}{2}}_1\right) + \Delta t A^{-1}\left(U^{n+\frac{1}{2}}_1\right)C\left(U^{n+\frac{1}{2}}_1\right) \tag{44c}$$

Table 1 Mechanical and thermal properties of α iron

ρ_0, kg/m^3	7.87×10^3	E, GPa	200	G, GPa	87
k, J/s · m · k	67.2	c_p, J/kg · k	440		

$$U^{n+1}_N = U^n_N - \frac{2\Delta t}{\Delta x}A^{-1}\left(U^{n+\frac{1}{2}}_N\right)B\left(U^{n+\frac{1}{2}}_N\right)\left(U^{n+\frac{1}{2}}_N - U^{n+\frac{1}{2}}_{N-\frac{1}{2}}\right) + \Delta t A^{-1}\left(U^{n+\frac{1}{2}}_N\right)C\left(U^{n+\frac{1}{2}}_N\right) \tag{44d}$$

It is seen that, rather than the centered difference, a one-sided spatial difference is employed in the preceding boundary techniques. This results in a first-order accuracy, which is less than the second-order interior finite difference technique. The truncation errors are propagated back into the interior. However, they have been found to not appreciably affect the overall accuracy of the difference scheme [29].

The stability analysis for the scheme depends on the characteristics of every equation. Therefore, the stability analysis will be addressed in the separate case studies. The finite difference code is implemented in Matlab.

B. Material Parameters

In the studies, pure iron is chosen as the material for numerical simulations. The conventional material properties of α iron are listed in Table 1.[‡]

The necessary information such as the initial dislocation density ρ_{d0}, Burgers's vector b, critical resolved stress τ_{cr0}, average dislocation line energy E_L, and reference resistance to dislocation motion k_{d0} are obtained accordingly from normal values for metals in [20].

$$\rho_{d0} = 10^{11}\ \text{m}^{-2}; \qquad b = 2.533\ \text{Å}; \qquad \tau_{\text{cr0}} = 300\ \text{MPa};$$
$$E_L = 0.207\ \text{Gb}^2; \qquad k_{d0} = 5 \times 10^5\ \text{N} \cdot \text{s/m}^3$$

Other required parameters related to dislocation are assumed. The relaxation time for dislocation motion t_d is assumed to be at the same level of viscous process. Hardening and softening coefficients $\tau_{c\rho}$ and $\tau_{c\theta}$ are chosen to be 1% of τ_{cr0}. The threshold value of dislocation density for hardening $\rho_{d\text{-HP}}$ is chosen to be $1.5 \times 10^3 \rho_{d0}$. The fraction factor for dislocation multiplication χ_L is set to be 0.8. The nondimensional effective coefficient ς for line tension is set to 0.8. The viscous drag coefficient B is set to 10^6 N · s/m^3.

$$t_d = 10^{-7}\ \text{s}; \qquad \tau_{c\rho} = 10^{-2}\tau_{\text{cr0}}; \qquad \tau_{c\theta} = -10^{-2}\tau_{\text{cr0}};$$
$$\rho_{d\text{-HP}} = 1.5 \times 10^3 \rho_{d0} \qquad \chi_L = 0.8; \qquad \varsigma = 0.8;$$
$$b_{\text{drag}} = 1 \cdot 10^6\ \text{N} \cdot \text{s/m}^3$$

At shock fronts, a large amount of dislocations are nucleated. Accordingly, the hardness and strength of the material is increased several times [13]. The model for the dislocation nucleation at the shock front is given by Eq. (6). It is assumed that dislocations start instantaneously to nucleate at shock fronts. The shock fronts can be identified by a sharp pressure gradient. The rate of nucleated dislocations at the shock front is given by

$$K_n = \frac{\chi_D}{E_L}W(P) = \frac{\chi_D}{E_L}(-P^e v_{i,i}) \tag{45}$$

where $\chi_D = 5 \times 10^{-4}$.

C. One-Dimensional Strain Case

This uniaxial strain problem yields only a nontrivial normal strain component ε_{yy}. It corresponds to a nontrivial velocity component v_y. Nontrivial stress components are σ_{yy}, σ_{xx}, and σ_{zz}. The governing equations can be written as follows.

$$\frac{\partial}{\partial t}\rho = -\rho\frac{\partial}{\partial y}v_y - v_y\frac{\partial}{\partial y}\rho \tag{46a}$$

[‡]Material property database available online at http://www.matweb.com [retrieved July 2002].

$$\rho\frac{\partial}{\partial t}v_y = -\rho v_y\frac{\partial}{\partial y}v_y + \frac{\partial}{\partial y}\sigma_{yy} \tag{46b}$$

$$\rho c_p\frac{\partial}{\partial t}\theta = -\rho c_p v_y\frac{\partial}{\partial y}\theta - \frac{\partial}{\partial y}q + k_d\rho_d b v_d v_d \tag{46c}$$

Among all the nonequilibrium processes, plastic flow is the dominant dissipative process. Therefore, the viscous process is not considered (i.e., $\sigma_{yy}^{\text{ne}} = 0$ and $\sigma_{xx}^{\text{ne}} = 0$). In Eq. (46c), the stored elastic strain energy by dislocations is not considered [i.e., $\varphi(\theta) = 0$], and the elastic thermal expansion is assumed to be small (i.e., $B = 0$). The kinematics are given by

$$\frac{\partial}{\partial y}v_y = V_{yy}^e + V_{yy}^{\text{plastic}} \tag{47a}$$

$$\frac{\partial}{\partial x}v_x = 0 = V_{xx}^e + V_{xx}^{\text{plastic}} \tag{47b}$$

where

$$V_{yy}^{\text{plastic}} = -\tfrac{1}{2}\rho_d b v_d \sin 2\phi \tag{47c}$$

$$V_{xx}^{\text{plastic}} = \tfrac{1}{2}\rho_d b v_d \sin 2\phi \tag{47d}$$

The constitutive relations are given by

$$\frac{\partial}{\partial t}\sigma_{xx} = -v_y\frac{\partial}{\partial y}\sigma_{xx} + \frac{E}{(1+\nu)(1-2\nu)}\left[(1-\nu)V_{xx}^e + \nu V_{yy}^e\right] \tag{48a}$$

$$\frac{\partial}{\partial t}\sigma_{yy} = -v_y\frac{\partial}{\partial y}\sigma_{yy} + \frac{E}{(1+\nu)(1-2\nu)}\left[\nu V_{xx}^e + (1-\nu)V_{yy}^e\right] \tag{48b}$$

$$t_q\frac{\partial}{\partial t}q = -t_q v_y\frac{\partial}{\partial y}q - q - k\frac{\partial}{\partial y}\theta \tag{48c}$$

$$\theta\frac{\partial}{\partial t}\rho_d = -v_y\frac{\partial}{\partial y}\rho_d + \frac{\chi_L(\theta)}{E_L}\left(\tau_{\text{ext}} - \frac{\varsigma Gb}{\Delta L} - Bv_d\right)v_d + K_n \tag{48d}$$

$$t_d\frac{\partial}{\partial t}v_d = -t_d v_y\frac{\partial}{\partial y}v_d - v_d + \frac{1}{k_d}\left(\tau_{\text{ext}} - \frac{\alpha Gb}{\Delta L} - Bv_d\right) \tag{48e}$$

$$\frac{\partial}{\partial t}\phi = -v_y\frac{\partial}{\partial y}\phi = 0 \tag{48f}$$

where the resolved external shear stress on the slip system is given by

$$\tau_{\text{ext}} = \tfrac{1}{2}(\sigma_{xx} - \sigma_{yy})\sin 2\phi \tag{49}$$

The critical stress for dislocation motions is given by Eq. (11). Substituting Eqs. (47a–47d) into Eqs. (48a) and (48b), we obtain

$$\begin{aligned}
\frac{\partial}{\partial t}\sigma_{xx} &= -v_y\frac{\partial}{\partial y}\sigma_{xx} + \frac{E}{(1+\nu)(1-2\nu)} \\
&\quad\times\left(-(1-2\nu)\frac{1}{2}\rho_d b v_d\sin 2\phi + \nu\frac{\partial}{\partial y}v_y\right) \\
\frac{\partial}{\partial t}\sigma_{yy} &= -v_y\frac{\partial}{\partial y}\sigma_{yy} + \frac{E}{(1+\nu)(1-2\nu)} \\
&\quad\times\left((1-2\nu)\frac{1}{2}\rho_d b v_d\sin 2\phi + (1-\nu)\frac{\partial}{\partial y}v_y\right)
\end{aligned} \tag{50}$$

The hydrostatic pressure P in this case is equal to $-(2\sigma_{xx} + \sigma_{yy})/3$. Initially, the 1-D strip is subjected to a uniform temperature distribution, and all the material points possess the same dislocation density.

$$\theta|_{t=0} = \theta_0; \qquad \rho_d|_{t=0} = \rho_{d0} \tag{51}$$

On the surface, a constant normal stress is applied. An adiabatic boundary is assumed.

$$\sigma(0, t \geq 0) = -\sigma_0; \qquad q(0,t) = 0 \tag{52}$$

Neglecting Eq. (48f), we have eight equations, as listed in Eqs. (46) and (48). If the system is written in the form of Eq. (39), we have

$$\begin{aligned}
&\boldsymbol{U} = \{\rho, v_y, \theta, \sigma_{xx}, \sigma_{yy}, q, \rho_d, v_d\}^T; \\
&\boldsymbol{A}(U) = \text{diag}\{1, \rho, \rho c_v, 1, 1, t_q, 1, t_d\} \\
&\boldsymbol{C}(U) = [0, 0, k_b\rho_d b v_d v_d, F_1, F_2, -q, F_3, F_4]^T \\
&\boldsymbol{B}(U) \\
&= \begin{bmatrix}
-v_y & -\rho & 0 & 0 & 0 & 0 & 0 & 0 \\
0 & -\rho v_y & 0 & 0 & 1 & 0 & 0 & 0 \\
0 & 0 & -\rho c_p v_y & 0 & 0 & -1 & 0 & 0 \\
0 & \frac{E\nu}{(1+\nu)(1-2\nu)} & 0 & -v_y & 0 & 0 & 0 & 0 \\
0 & \frac{E(1-\nu)}{(1+\nu)(1-2\nu)} & 0 & 0 & -v_y & 0 & 0 & 0 \\
0 & 0 & -k & 0 & 0 & -t_q v_y & 0 & 0 \\
0 & 0 & 0 & 0 & 0 & 0 & -v_y & 0 \\
0 & 0 & 0 & 0 & 0 & 0 & 0 & -t_d v_y
\end{bmatrix}
\end{aligned} \tag{53}$$

where

$$\begin{aligned}
F_1 &= \frac{E}{2(1+\nu)}(\rho_d b v_d \sin 2\phi); \qquad F_2 = -F_1; \\
F_3 &= \frac{\chi(\theta)}{E_L}\left(\frac{1}{2}(2\sigma_{xx}^e - \sigma_{yy}^e)\sin 2\phi - \frac{\alpha Gb}{\Delta L}\right)v_d + K_n; \\
F_4 &= -v_d + \frac{1}{k_d}\left(\frac{1}{2}(2\sigma_{xx}^e - \sigma_{yy}^e)\sin 2\phi - \frac{\alpha Gb}{\Delta L}\right)
\end{aligned}$$

There are various propagations or relaxations of σ_{xx}, v_y (or σ_{yy}), θ, ρ_d, and v_d. Each of these has a different characteristic speed. The associated stability conditions can be written as follows [27,28].

$$\begin{aligned}
&|v_y|\frac{\Delta t}{\Delta x} \leq 1; \qquad \left(|v_y| + \sqrt{\frac{E(1-\nu)}{\rho(1+\nu)(1-2\nu)}}\right)\frac{\Delta t}{\Delta x} \leq 1; \\
&\left(|v_y| + \sqrt{\frac{k}{\rho c_v}}\right)\frac{\Delta t}{\Delta x} \leq 1; \qquad \left(|v_y| + \sqrt{\frac{\kappa\rho}{t_g}}\right)\frac{\Delta t}{\Delta x} \leq 1
\end{aligned} \tag{54}$$

The individual sufficient stability condition requires a different time step. Therefore, at each calculation step, the following time step is chosen as the smallest time step among all the imposed time steps.

$$\Delta t = \min\left\{\frac{\Delta x}{|v_y|}, \frac{\Delta x}{(|v_y| + \sqrt{\frac{E(1-\nu)}{\rho(1+\nu)(1-2\nu)}})}, \frac{\Delta x}{(|v_y| + \sqrt{\frac{k}{\rho c_v}})}, \frac{\Delta x}{(|v_y| + \sqrt{\frac{\kappa\rho}{t_g}})}\right\} \tag{55}$$

The finite difference procedure, finite difference code, and boundary techniques are first tested by using selected simple cases. The top surface of the 1-D strip is subjected to a constant normal stress σ_0. The stress σ_0 is applied from $t = 0$. The applied loading is low enough to avoid complication.

1. Test Study: $\sigma_0 = 1$ GPa *and* $\phi = 0$ deg

To test the numerical scheme and stability criteria, we choose the orientation of the slip system ϕ to be 0 deg. Then the resolved shear stress on the slip system is zero. It leads to elimination of plastic flow. The elastic wave speed is calculated as 5845.9 m/s, which is close to the elastic (uniaxial strain) wave in α iron; that is,

$$\sqrt{\frac{E_1(1-\nu)}{\rho_0(1+\nu)(1-2\nu)}}$$

It is observed that there is some overshoot at the wave front. This overshoot is induced by the error transmitted from the boundary technique. An artificial viscosity is added to damp this overshoot. A quadratic form gives the pseudoviscous normal stress σ^v.

$$\sigma^v = \begin{cases} \rho(a\Delta y)^2 \frac{\partial^2 v_y}{\partial y^2} & \text{if } \frac{\partial v_y}{\partial y} < 0 \\ 0 & \text{if } \frac{\partial v_y}{\partial y} < 0 \end{cases} \tag{56}$$

It is found that by choosing the pseudoviscous parameter a in Eq. (56) to a value of 2, the artificial viscosity damped the overshoot,

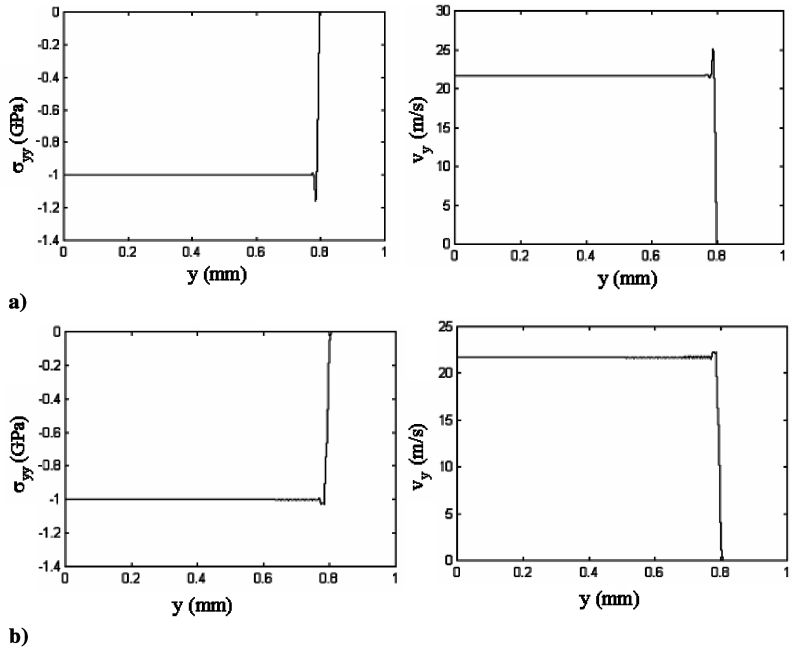

Fig. 4 Elastic compression wave for $\sigma_0 = 1$ GPa, $\phi = 0$ deg, at time $t = 1.3486 \times 10^{-7}$ s: a) without artificial viscosity ($a = 0$) and b) with artificial viscosity ($a = 2$).

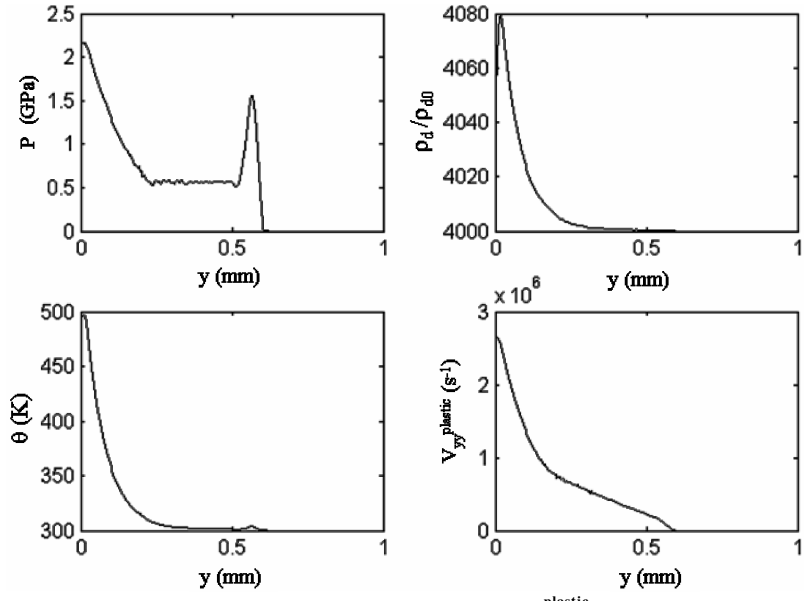

Fig. 5 Profiles of pressure P, temperature θ, dislocation density ρ_d, and plastic flow V_{yy}^{plastic}, at time $t = 96$ ns for $\sigma_0 = 4$ GPa and $\phi = 45$ deg.

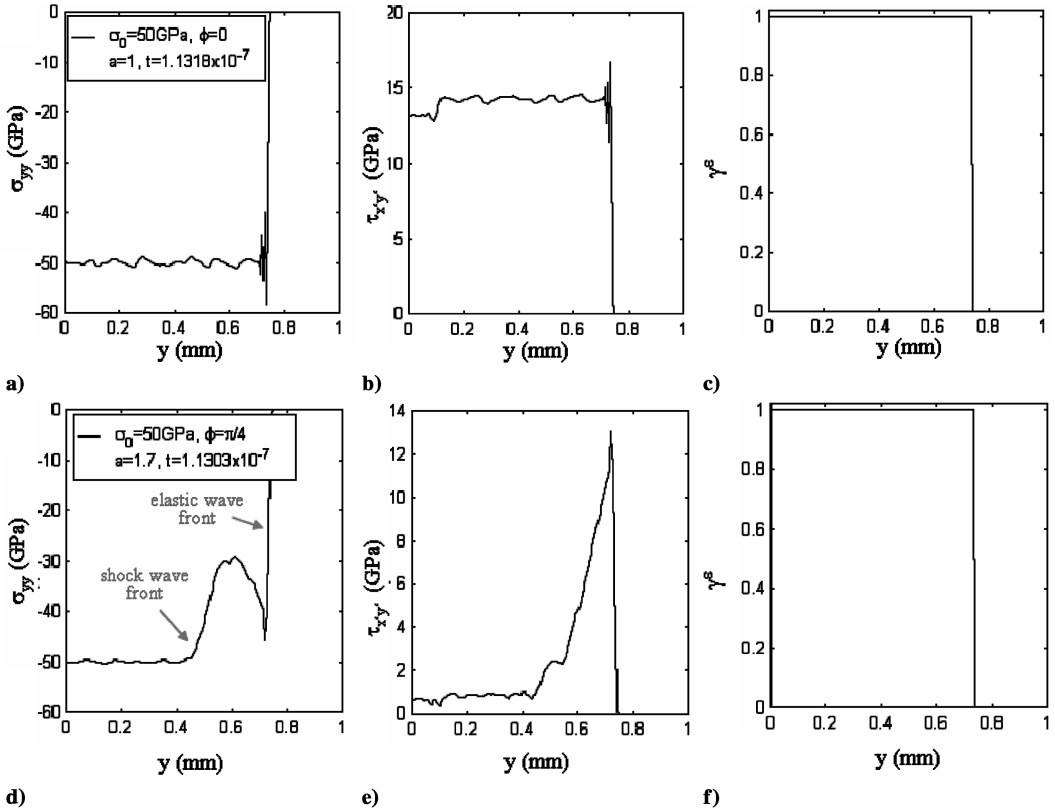

Fig. 6 Wave profiles of normal stress σ_{yy}, maximum shear stress $\tau_{x'y'}$, and mass fraction of ε phase ${}^{\varepsilon}\gamma$ for $\sigma_0 = 50$ GPa with a–c) $\phi = 0$ deg at $t = 1.1318 \times 10^{-7}$ s; d–f) $\phi = 45$ deg at $t = 1.1303 \times 10^{-7}$ s.

and simultaneously the sharpness of shock front is slightly relaxed (Fig. 4).

2. Localized Plastic Flow and Heating: $\sigma_0 = 4$ GPa and $\phi = 45$ deg

The applied loading $\sigma_0 = 4$ GPa. The results are shown in Fig. 5. A localized heating zone close to the loading surface $y = 0$ is observed. A large amount of plastic flow and the associated dislocation accumulation in the same zone are also observed.

3. Strong Shock: $\sigma_0 = 50$ GPa

With this strong shock, the resulting hydrostatic pressure P is much larger than the critical pressure $P_{\text{cr}} = 11.3$ GPa for $\alpha \to \varepsilon$ iron phase transition. The phase transition model used in this paper can be referred to in [26]. We considered two cases: one with $\phi = 0$ deg and the second with $\phi = 45$ deg. In the first case, there is no generated plastic flow. The profile of normal stresses σ_{yy}, the maximum shear stress $\tau_{x'y'} = (\sigma_{xx} - \sigma_{yy})/2$, and the mass fraction of ε phase ${}^{\varepsilon}\gamma$ are shown in Figs. 6a–6c at time $t = 1.1318 \times 10^{-7}$ s. It is shown that as the shock wave front passes through, the phase transition takes place almost instantly. The phase transition front, which is indicated by a sharp front in Fig. 6c, is only slightly behind the shock wave front. The propagation speed of the shock wave is calculated as 6538.0 m/s, which is close to the elastic (uniaxial strain) wave speed in ε iron. Because the ε iron is harder than the α iron, the speed of the elastic wave of ε iron is faster than that of α iron. Then the second wave of a larger speed, generated by phase transition, overtakes the first wave of a slower speed. However, we can see that the sudden change of the mechanical properties through the process of phase transition induces oscillations to all the profiles.

In a second case, to generate plastic flow, the slip system is set at 45 deg to the x axis. Similarly, the profiles of σ_{yy}, the maximum shear stress $\tau_{x'y'}$, and the mass fraction of ε phase ${}^{\varepsilon}\gamma$ are shown in Figs. 6d–6f at time $t = 1.1303 \times 10^{-7}$ s. It is also observed that just after the shock front passes, $\alpha \to \varepsilon$ phase transition takes place almost instantly. The phase transition front is indicated by a sharp front in Fig. 6f. Unlike the first case, the wave profiles exhibit a two-wave structure (Fig. 6d). The first wave, which has a sharp front, is identified as the elastic shock wave of ε iron. Its wave speed is about 6511.6 m/s. The second wave is generated by associated plastic flows and has a dispersive wave front. In comparison with the first case with no plastic flow ($\phi = 0$ deg), it is observed that plastic waves increase densities and particle velocities in the range of plastic waves. Also, the maximum shear stress $\tau_{x'y'} = (\sigma_{xx} - \sigma_{yy})/2$, as shown in Fig. 7e, is brought down from a value of 13 GPa at the shock front, which accounts for hardening effects and is about 45 times the initial yielding stress τ_{cr0}, to the level of the initial yielding stress τ_{cr0} after the shock passes.

D. Two-Dimensional Half-Space Case

For the 2-D half-space problem (Fig. 2a), there are two nontrivial velocity components: v_x and v_y. The nontrivial stress components are σ_{yy} (or σ^e) and τ_{xy} (or t^e). Other state variables follow the same descriptions as in the previous case. The governing equations can be written as follows.

$$\begin{cases} \frac{\partial}{\partial t}\rho = -\rho \frac{\partial}{\partial y} r_y - r_y \frac{\partial}{\partial y}\rho \\ \rho \frac{\partial}{\partial t} v_x = -\rho v_y \frac{\partial}{\partial y} v_x + \frac{\partial}{\partial y}\tau^e \\ \rho \frac{\partial}{\partial t} v_y = -\rho v_y \frac{\partial}{\partial y} v_y + \frac{\partial}{\partial y}\sigma^e \\ \rho c_p \frac{\partial}{\partial t}\theta = -\rho c_p v_y \frac{\partial}{\partial y}\theta - \frac{\partial}{\partial y} q + k_d \rho_d b v_d \nabla_d \end{cases} \tag{57}$$

Following the same arguments as in the previous 1-D strip case, the constitutive relations are given by

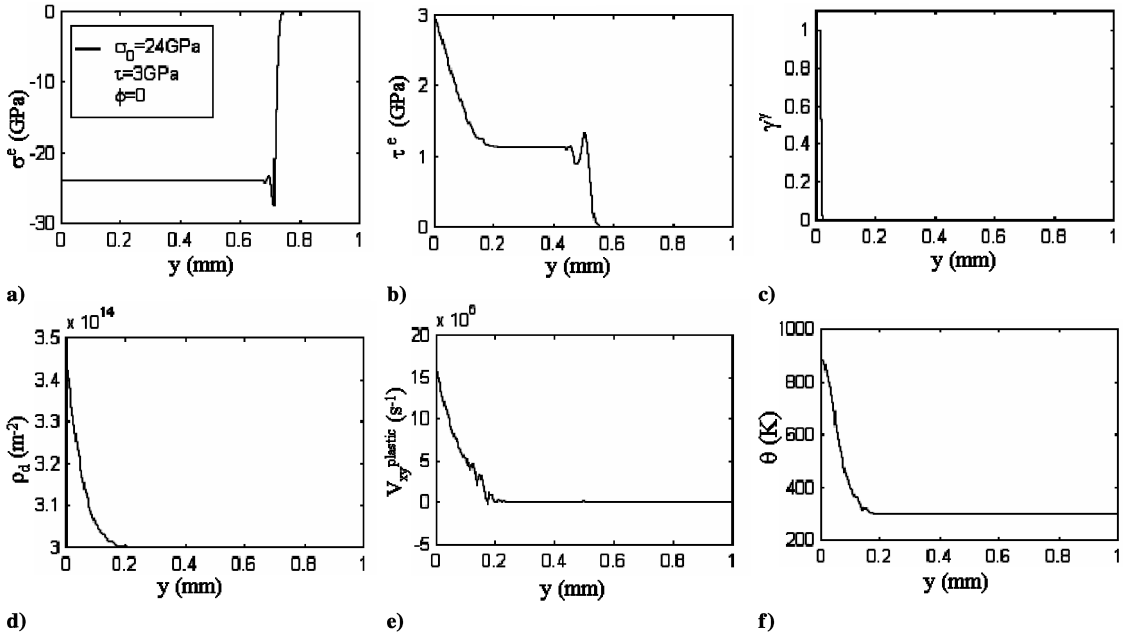

Fig. 7 Profiles of normal stress σ^e, shear stress τ^e, mass fraction of γ phase iron ${}^{\gamma}\gamma$, dislocation density ρ_d, plastic flow V_{xy}^{plastic}, and temperature θ at time $t = 1.3856 \times 10^{-7}$ s for $\sigma_0 = 24$ GPa, $\tau_0 = 3$ GPa, and $\phi = 0$ deg.

$$
\begin{cases}
\frac{\partial}{\partial t}\tau^e = -v_y \frac{\partial}{\partial y}\tau^e + \mathrm{G}\frac{\partial}{\partial y}v_x - G\rho_d b v_d \cos 2\phi \\
\frac{\partial}{\partial t}\sigma^e = -v_y \frac{\partial}{\partial y}\sigma^e + E\frac{\partial}{\partial y}v_y - \frac{1}{2}E\rho_d b v_d \sin 2\phi \\
t_q \frac{\partial}{\partial t} q = -t_q v_y \frac{\partial}{\partial y} q - q - k\frac{\partial}{\partial y}\theta \\
\frac{\partial}{\partial t}\rho_d = -v_y \frac{\partial}{\partial y}\rho_d + \frac{\chi(\theta)}{E_L}\left(-\frac{1}{2}\sigma^e \sin 2\phi + \frac{1}{2}\tau^e \cos 2\phi - \frac{\alpha G b}{\Delta L}\right) v_d + k_n \\
t_d \frac{\partial}{\partial t} v_d = -t_d v_y \frac{\partial}{\partial y} v_d - v_d + \frac{1}{k_d}\left(-\frac{1}{2}\sigma^e \sin 2\phi + \frac{1}{2}\tau^e \cos 2\phi - \frac{\alpha G b}{\Delta L}\right) \\
\frac{\partial}{\partial t}\phi = -v_y \frac{\partial}{\partial y}\phi + \frac{\partial}{\partial y} v_x
\end{cases}
\tag{58}
$$

Comparing to the 1-D strip case, an extra boundary condition is provided.

$$\tau(0, t \geq 0) = \tau_0 \tag{59}$$

The stability conditions for the finite difference scheme can be obtained.

$$
\begin{gathered}
|v_y|\frac{\Delta t}{\Delta x} \leq 1; \qquad \left(|v_y| + \sqrt{\frac{E}{\rho}}\right)\frac{\Delta t}{\Delta x} \leq 1; \\
\left(|v_y| + \sqrt{\frac{G}{\rho}}\right)\frac{\Delta t}{\Delta x} \leq 1; \qquad \left(|v_y| + \sqrt{\frac{k}{\rho c_v}}\right)\frac{\Delta t}{\Delta x} \leq 1
\end{gathered}
\tag{60}
$$

In comparison with the 1-D strain problem, a normal stress σ_0 and a shear stress τ_0 are applied to the top surface of the half-space. Therefore, two sets of waves are created: one corresponding to compression waves and the other to shear waves. The plastic flows are generated by the activation and the evolutions of the dislocation slip system. Afterward, the aforementioned thermal softening effects and the hardening effects compete with each other.

1. Localized Plastic Flow: $\sigma_0 = 24$ GPa, $\tau_0 = 3$ GPa, and $\phi = 0$ deg

The applied shear stress τ_0 is 10 times the initial critical yielding stress τ_{cr0}, whereas the applied normal stress σ_0 is kept small at 24 GPa to impede the $\alpha \rightarrow \varepsilon$ phase transition. The profiles of normal stress σ^e, shear stress τ^e, dislocation density ρ_d, plastic flow V_{xy}^{plastic}, temperature θ, and mass fractions of γ phase iron ${}^{\gamma}\gamma$ at time $t = 1.3856 \times 10^{-7}$ s are shown in Figs. 7a–7f. The speed of compression wave is calculated as 5138.7 m/s (Fig. 7a), which is close to that of the elastic (uniaxial stress) wave for α iron given by $\sqrt{E_1/\rho_0}$. The shear wave generates plastic flows. Thus, the shear waves have a two-wave structure with a very dispersive plastic wave (Fig. 7b). The speed of the shear wave is calculated as 3695.2 m/s, which is a little bit larger than that of the shear wave for α iron given by $\sqrt{\mathrm{G}_1/\rho_0} = 3324.9$ m/s. As observed in Figs. 7d–7f, the accumulation of plastic flow, dislocation density, and heating is only restricted to a narrow region close to the half-space surface and far behind the shear wave front. The maximum temperature is larger than 800 K, which is high enough to set off $\alpha \rightarrow \gamma$ phase transition, with a combined loading condition. However, the amount of time required for accumulating the necessary heat delays the $\alpha \rightarrow \gamma$ phase transition. Then the front of $\alpha \rightarrow \gamma$ phase transition is far behind the shear wave front (Fig. 7c).

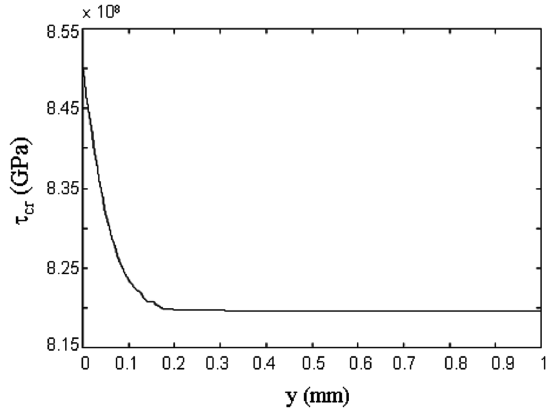

Fig. 8 Profiles of the critical stress τ_{cr} at time $t = 1.3856 \times 10^{-7}$ s for $\sigma_0 = 24$ GPa, $\tau_0 = 3$ GPa, and $\phi = 0$ deg.

Meanwhile, the hardening due to dislocation nucleation and accumulations has been identified by the increase of critical stress in the region of highest dislocation density, as shown in Fig. 8. The competition of the thermal softening effects and the hardening effects results in some discontinuities or oscillations in the distribution of dislocation motion, as shown in Fig. 7e.

VIII. Conclusions

We formulated a deterministic dislocation-based plasticity model that can account for the formation of dislocation behind a shock front, dislocation pileup, dislocation release, and localized heating at high strain rates. The formulation is in a hybrid framework of internal state variables and thermodynamic fluxes or extended nonequilibrium state variables. The combination of the second law of thermodynamics and the formulated constitutive relations provide expressions for the specific entropy and change of temperature due to different irreversible mechanisms. An application demonstrates the phenomena of localized heating.

Appendix A: Dislocation Multiplication and Dislocation Reactions

In 1950, Frank and Reed suggested an explanation of dislocation multiplication based on dislocation loops formed by pinned dislocations. As the applied shear stress reaches a critical stress, which corresponds to a dislocation loop with a critical radius as half of the distance between dislocations, the dislocation loop becomes unstable and starts to expand. This expansion results in new dislocations to reduce the high stored energy in the expanded loop [17,22,30]. We follow a phenomenological model by Hähner [21]. It assumes that the dislocation multiplication is proportional to a fraction of plastic work by the dislocation loop expansion.

$$K_m^{(\alpha)} = \frac{\chi_L^{(\alpha)}(\theta)}{E_L}\rho_d^{(\alpha)} b^{(\alpha)} v^{(\alpha)} \tau_{\text{eff}}^{(\alpha)} \tag{A1}$$

where E_L is the average dislocation line energy over all the slip systems, $\chi_L^{(\alpha)}$ is the fraction of plastic work that contributes to the formation of dislocation segments (α) ($\chi_L^{(\alpha)}$ depends on temperature θ), and $\tau_{\text{eff}}^{(\alpha)}$ is the local resolved shear stress acting on dislocation segments in slip system (α) [Eq. (8)].

The reaction [22,23] between dislocation segments of two different slip systems may lead to the formation of a junction segment of a new slip system with a new Burgers vector. At the same time, the motion of dislocation segments may break the existing junctions. Therefore, the rate of change of the dislocation segments of slip system (α) is written as

$$K_J^{(\alpha)} = -K_{J-}^{(\alpha)} + K_{J+}^{(\alpha)} \tag{A2}$$

where the loss rate of dislocation segments in slip system (α), $K_{J-}^{(\alpha)}$, due to their reaction with dislocation segments of slip system (β), is written as follows.

$$K_{J-}^{(\alpha)} = -\frac{1}{\sqrt{\rho_d}}\sum_{\beta}[R_F^{(\alpha)(\beta)}(v^{(\alpha)} + v^{(\beta)}) + R_B^{(\alpha)(\beta)} v^{(\beta)}]\rho_d^{(\alpha)}\rho_d^{(\beta)} \tag{A3}$$

where $R_F^{(\alpha)(\beta)}$ is the probability that two dislocation segments of slip systems (α) and (β) react and form a new slip system, whereas $R_B^{(\alpha)(\beta)}$ is the probability for a dislocation segment on slip system (β) to break a junction of slip system (α); ρ_d is the average dislocation density in a infinitesimal volume, which is,

$$\rho_d = \sum_{\alpha}\rho_d^{(\alpha)} \tag{A4}$$

The rate of dislocation formation for a slip system (α), $K_{J+}^{(\alpha)}$, caused by junction formation and breaking, is given by

$$K_{J+}^{(\alpha)} = \frac{1}{\sqrt{\rho_d}}\sum_{\beta 2}\sum_{\beta 1} R_c^{(\alpha)(\beta 1)(\beta 2)} v^{(\beta 1)} v^{(\beta 2)} \rho_d^{(\beta 1)} \rho_d^{(\beta 2)} \tag{A5}$$

where $R_c^{(\alpha)(\beta 1)(\beta 2)}$ is the construction probability of dislocation segments of slip system (α) due to the reaction between dislocation segments of slip systems ($\beta 1$) and ($\beta 2$). The nondimensional quantities $R_F^{(\alpha)(\beta)}$, $R_B^{(\alpha)(\beta)}$, and $R_c^{(\alpha)(\beta 1)(\beta 2)}$ are material parameters. They have to be obtained by measurement or computer simulation of junction processes [22,23].

Appendix B: Contributions to the Resolved Shear Stress

We assume the ensemble of spatially fluctuating short- and long-range interactions between dislocation segments to be zero, although it can be easily added by a nonlocal kernel [22]. The external resolved shear stress is related to the macroscopic stress tensor by the Peach–Koehler formula [19,25,31],

$$\tau_{\text{ext}}^{(\alpha)} = \sigma_{ij} Z_{ij}^{(\alpha)} \tag{B1}$$

The internal stress may be described by a line tension approximation [17,22,25]; that is,

$$\tau_{\text{int}}^{(\alpha)} = \frac{\varsigma^{(\alpha)} G b^{(\alpha)}}{\Delta L} \tag{B2}$$

where $\varsigma^{(\alpha)}$ is the nondimensional effective coefficient, G is the average shear modulus of crystal, $b^{(\alpha)}$ is the magnitude of the Burgers vector, and ΔL is the averaged distance between the two closest dislocation segments. Obviously, ΔL decreases as the average dislocation density ρ_d increases. It is assumed

$$\Delta L = \frac{1}{\sqrt{\rho_d}} \tag{B3}$$

The drag mechanisms on dislocation motions are due to the relaxation effects during the interaction of dislocations with phonons and electrons and are also due to the relaxation effects in the dislocation core [13]. For metals at high temperature, phonon drag is the dominant drag mechanism; at low temperature, electron drag is the major mechanism [13]. To a first approximation, a Newtonian viscous model is used for these drag effects; that is,

$$\tau_{\text{drag}}^{(\alpha)} = \mathrm{B}_{\text{drag}}^{(\alpha)} \mathrm{v}^{(\alpha)} \tag{B4}$$

where $B_{\text{drag}}^{(\alpha)}$ is the viscous drag coefficient, which can be a function of the dislocation motion.

Acknowledgments

We would like to acknowledge and thank the U.S. Air Force Office of Scientific Research (AFOSR), the U.S. Air Force Research Laboratory Munitions Directorate (AFRL/MN) and the University of Florida for the support on the research projects. Specifically, we would like to thank the AFOSR project technical monitors Dean Mook and Craig Hartley, and AFRL technical monitor Mary (Molly) L. Hughes.

References

[1] Forrestal, M. J., Frew, D. J., Honchak, S. J., and Brar, N. S., "Penetration of Ground and Concrete Targets with Ogive-Nose Steel Projectiles," *International Journal of Impact Engineering*, Vol. 18, No. 5, 1996, pp. 465–476. doi:10.1016/0734-743X(95)00048-F

[2] Frew, D. J., Hanchak, S. J., Green, M. L., and Forrestal, M. J., "Penetration of Concrete Targets with Ogive-Nose Steel Rods," *International Journal of Impact Engineering*, Vol. 21, No. 6, 1998, pp. 489–497. doi:10.1016/S0734-743X(98)00008-6

[3] Zener, C., "Stress Induced Preferential Ordering of Pairs of Solute Atoms in Metallic Solid Solution," *Physical Review*, Vol. 71, No. 1, 1947, pp. 34–38. doi:10.1103/PhysRev.71.34

[4] Boley, B. A., and Weiner, J. H., *Theory of Thermal Stresses*, Wiley, New York, 1960.

[5] Bishop, J. E., and Kinra, V. K., "Thermoelastic Damping of a laminated Beam in Flexure and Extension," *Journal of Reinforced Plastics and Composites*, Vol. 12, No. 2, 1993, pp. 210–226. doi:10.1177/073168449301200207

[6] Bishop, J. E., Kinra, V. K., and Milligan, B. K., "Elastothermodynamic

Damping in Metal-Matrix Composites," *Metal Matrix Composites (ICCM/9)*, Vol. 1, International Committee on Composite Materials, Tours, France, July 1993, pp. 311–318.

[7] Maugin, G. A., *The Thermomechanics of Plasticity and Fracture*, Cambridge Univ. Press, Cambridge, England, U.K., 1992.

[8] Rosakis, P., Rosakis, A. J., Ravichandran, G., and Hodowany, J., "A Thermodynamic Internal Variable Model for Partition of Plastic Work into Heat and Stored Energy in Metals," *Journal of the Mechanics and Physics of Solids*, Vol. 48, No. 3, 2000, pp. 581–607. doi:10.1016/S0022-5096(99)00048-4

[9] Makowski, J., and Stumpf, H., "Thermodynamically Based Concept for the Modeling of Continua with Microstructure and Evolving Defects," *International Journal of Solids and Structures*, Vol. 38, Nos. 10–13, 2001, pp. 1943–1961. doi:10.1016/S0020-7683(00)00145-1

[10] Hartley, C. S., "A Method for Linking Thermally Activated Dislocation Mechanisms of Yielding with Continuum Plasticity Theory," *Philosophical Magazine*, Vol. 83, Nos. 31–34, 2003, pp. 3783–3808. doi:10.1080/14786430310001599522

[11] Gurtin, M. E., "On the Plasticity of Single Crystals: Free Energy, Microforces, Plastic-Strain Gradients," *Journal of the Mechanics and Physics of Solids*, Vol. 48, No. 5, 2000, pp. 989–1036. doi:10.1016/S0022-5096(99)00059-9

[12] Forest, S., Sievert, R., and Aifantis, E. C., "Strain Gradient Crystal Plasticity: Thermomechanical Formulation and Applications," *Journal of the Mechanical Behavior of Materials*, Vol. 13, Nos. 3–4, 2002, pp. 219–232.

[13] Meyers, M. A., *Dynamic Behavior of Material*, Wiley, New York, 1994.

[14] Armstrong, R. W., and Zerilli, F. J., "Dislocation Mechanics Aspects of Plastic Instability and Shear Banding," *Mechanics of Materials*, Vol. 17, Nos. 2–3, 1994, pp. 319–327. doi:10.1016/0167-6636(94)90069-8

[15] Jou, D., Casas-Vazquez, J., and Lebon, G., *Extended Irreversible Thermodynamics*, Springer, New York, 1996.

[16] Jou, D., Casas-Vazquez, J., and Lebon, G., "Recent Bibliography on Extended Irreversible Thermodynamics and Related Topics (1995–1998)," *Journal of Non-Equilibrium Thermodynamics*, Vol. 23, No. 3, 1998, pp. 277–297.

[17] Hutchison, T. S., and Baird, D. C., *The Physics of Engineering Solids*, Wiley, New York, 1967.

[18] Klassen-Neklyudova, M. V., *Plasticity of Crystals*, Consultants Bureau Enterprises, New York, 1962.

[19] Needleman, A., and van der Giessen, E., "Discrete Dislocation and Continuum Descriptions of Plastic Flow," *Materials Science and Engineering A*, Vol. 309–310, July 2001, pp. 1–13. doi:10.1016/S0921-5093(00)01684-1

[20] Hull, D., and Bacon, D. J., *Introduction to Dislocations*, 4th ed., Butterworths–Heinemann, Oxford—Boston, 2001.

[21] Hähner, P., "On the Foundations of Stochastic Dislocation Dynamics," *Applied Physics A: Materials Science and Processing*, Vol. 62, No. 5, 1996, pp. 473–481. doi:10.1007/BF01567120

[22] Zaiser, M., "Statistical Modeling of Dislocation Systems," *Materials Science and Engineering A*,Vol. 309–310, July 2001, pp. 304–315. doi:10.1016/S0921-5093(00)01676-2

[23] El-Azab, A., "Statistical Mechanics Treatment of the Evolution of Dislocation Distributions in Single Crystals," *Physical Review B*, Vol. 61, No. 18, 2000, pp. 11 956–11 966. doi:10.1103/PhysRevB.61.11956

[24] Politano, O., and Salazar, J. M., "A 3-D Mesoscopic Approach for Discrete Dislocation Dynamics," *Materials Science and Engineering A*, Vol. 309–310, July 2001, pp. 261–264. doi:10.1016/S0921-5093(00)01765-2

[25] Verdier, M., Fivel, M., and Groma, I., "Mesoscopic Scale Simulation of Dislocation Dynamics in FCC Metals: Principles and Applications," *Modelling and Simulation in Materials Science and Engineering*, Vol. 6, No. 6, 1998, pp. 755–770. doi:10.1088/0965-0393/6/6/007

[26] Lu, X., "Nonequilibrium Thermodynamic Models for the Dynamic Behavior of Polycrystalline Solids," Ph.D. Thesis, School of Aerospace Engineering, Georgia Inst. of Technology, Atlanta, GA, 2002.

[27] Richtmyer, R. D., and Morton, K. W., *Difference Methods for Initial-Value Problems*, 2nd ed., Interscience, New York, 1967.

[28] Durran, D. R., *Numerical Methods for Wave Equations in Geophysical Fluid Dynamics*, Springer, New York, 1999.

[29] Latham, R. L., Jr., "Interaction of Stress Waves and Cracks Using a Second Order Accurate Finite Difference Method," Ph.D. Thesis, School of Aerospace Engineering, Georgia Inst. of Technology, Atlanta, GA, 1982.

[30] Guinier, A., and Jullien, R., "The Solid State from Superconductors to Superalloys," *International Union of Crystallography*, Oxford Univ. Press, Oxford, 1989.

[31] Van der Giessen, E., and Needleman, A., "Discrete Dislocation Plasticity: A Simple Planar Model," *Modelling and Simulation in Materials Science and Engineering*, Vol. 3, No. 5, 1995, pp. 689–735. doi:10.1088/0965-0393/3/5/008

T. Nicholas
Associate Editor